Cell Systems
Perspective

Why Do Fast-Growing Bacteria Enter Overflow Metabolism? Testing the Membrane Real Estate Hypothesis

Mariola Szenk,[1,2] Ken A. Dill,[1,3] and Adam M.R. de Graff[1,*]
[1]Laufer Center for Physical and Quantitative Biology, Stony Brook University, Stony Brook, NY, USA
[2]Department of Biomedical Engineering, Stony Brook University, Stony Brook, NY, USA
[3]Departments of Chemistry, and Physics and Astronomy, Stony Brook University, Stony Brook, NY, USA
*Correspondence: adam.degraff@stonybrook.edu
http://dx.doi.org/10.1016/j.cels.2017.06.005

Bacteria and other cells show a puzzling behavior. At high growth rates, *E. coli* switch from respiration (which is ATP-efficient) to using fermentation for additional ATP (which is inefficient). This *overflow metabolism* results in a several-fold decrease in ATP produced per glucose molecule provided as food. By integrating diverse types of experimental data into a simple biophysical model, we give evidence that this onset is the result of the *membrane real estate hypothesis*: Fast growth drives cells to be bigger, reducing their surface-to-volume ratios. This decreases the membrane area available for respiratory proteins despite growing demand, causing increased crowding. Only when respiratory proteins reach their crowding limit does the cell activate fermentation, since fermentation allows faster ATP production per unit membrane area. Surface limitation thus creates a Pareto trade-off between membrane efficiency and ATP yield that links metabolic choice to the size and shape of a bacterial cell. By exploring the predictions that emerge from this trade-off, we show how consideration of molecular structures, energetics, rates, and equilibria can provide important insight into cellular behavior.

A major priority of a cell is obtaining and managing its energy. Many cells show a puzzling behavior. On the one hand, in dilute glucose environments with ample oxygen, many organisms obtain their energy almost exclusively from aerobic respiration. In this process, glucose is fully oxidized by glycolysis and the tricarboxylic acid (TCA) cycle, with the captured energy used by the electron transport chain to make ATP. On the other hand, in concentrated glucose environments, *Escherichia coli* and other organisms switch and obtain some of their energy anaerobically (without using oxygen) by acetate fermentation, even when oxygen is plentiful (Farmer and Jones, 1976; Kayser et al., 2005; Vemuri et al., 2006; Vazquez et al., 2008; Molenaar et al., 2009; Zhuang et al., 2011; Valgepea et al., 2011, 2013; Peebo et al., 2015; Basan et al., 2015). This so-called overflow metabolism is puzzling because acetate fermentation produces far fewer ATP per glucose molecule than respiration does (Neidhardt and Curtiss, 1996). Why should fast-growing cells switch to a more inefficient mechanism of energy utilization? Does the cell become driven by some fitness objective that does not require efficient production of energy?

Various explanations have been proposed for the onset of overflow metabolism. These include the hypothesis that it results from the repression of the TCA cycle (Vemuri et al., 2006; Nahku et al., 2010) or acetate recycling enzymes (Nahku et al., 2010), possibly due to catabolite repression (Nahku et al., 2010). Others propose that fermentation is preferred at high growth rates due to its lower biosynthesis cost relative to the electron transport chain (Basan et al., 2015). Finally, some propose that respiration is limited due to the finite space within the inner membrane, where the electron transport chain is located (Andersen and Meyenburg, 1980; Zhuang et al., 2011).

Different modeling approaches have been used to test these hypotheses. One approach entails flux-balance models, which treat the detailed stoichiometry of metabolic reactions (Vazquez et al., 2008, 2010; O'Brien et al., 2013; van Rijsewijk et al., 2011; Valgepea et al., 2011; Zhuang et al., 2011; Feist et al., 2007). Given a set of input constraints such as maximal glucose uptake and oxygen consumption, these models predict the fluxes that optimize an objective-like growth rate. Another approach is more coarse-grained in having many fewer components, for example dividing all the proteins in the proteome into a few classes, for the purpose of exploring principles, such as the optimal allocation of the proteome (Molenaar et al., 2009; Basan et al., 2015). Yet another approach, which does not treat the spatial aspects per se, focuses on speed versus efficiency of metabolic pathways (Flamholz et al., 2013; Noor et al., 2014). However, in common among these models is their neglect of structural properties of the individual proteins, such as their physical sizes, shapes, and packing, and the forces that partition them between the bulk and the membrane.

Here, we approach the problem of overflow metabolism in *E. coli* using such considerations. We consider the hypothesis that membrane space can become too limited for a cell to "breathe enough," called the "membrane economics hypothesis" by Mahadevan (Zhuang et al., 2011). Although it is just terminology, we prefer a slightly different term—*the membrane real estate hypothesis*—to make clear that the constraint is on lateral space in the membrane, not on costs in energy or biomass. To test this hypothesis, we use experimental data on cell length and width to demonstrate that the packing of the electron transport chain and other inner membrane proteins reaches its limit concurrently with the onset of overflow metabolism.

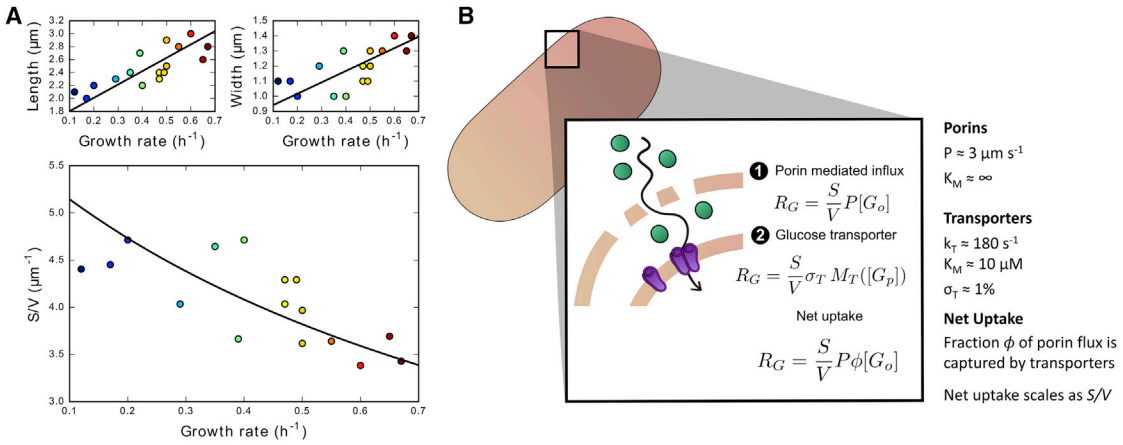

Figure 1. Mechanism of Glucose Uptake

(A) The surface-to-volume (*S*/*V*) ratio decreases with growth rate due to changes in cell length and cell width, in conflict with the cell's increasing demand for membrane space (Volkmer and Heinemann, 2011).

(B) Glucose uptake is a two-step process in which diffusion through outer membrane porins is followed by active uptake through inner membrane transporters modeled by the Michaelis-Menten function $M_T([G_p])$. While outer membrane influx is proportional to external glucose concentration $[G_o]$, inner membrane uptake is dependent on periplasmic glucose concentration $[G_p]$. We relate these through the factor ϕ. The total uptake per cell volume scales with *S*/*V* of the cell.

Furthermore, we derive respiration capacity from molecular kinetic data and show that the capacity of the electron transport chain to generate ATP is saturated as it reaches a concentration at which the membrane runs out of space. Finally, we show that the membrane real estate model predicts the steep rise in the [NADH]/[NAD^+] ratio observed prior to the onset of fermentation. The model thus suggests that overflow metabolism is triggered by membrane crowding to avoid NADH imbalance (Vemuri et al., 2006). By bringing together multiple types of data—on protein structures, energy balance, and rates and equilibria—we make a plausibility case for the triggering of overflow metabolism.

Our modeling of *E. coli* metabolism begins from two basic assumptions. First, we assume the cell's capacity to produce energy is proportional to the cell membrane surface area *S*, since this physically limits the cell's glucose uptake and respiratory capacity under the conditions studied here. Second, we assume the cell's rate of energy demand is proportional to the cell's volume *V* at a given growth rate, because expenditures are mostly on the synthesis required to replicate a cell. Under steady-state growth conditions, the cell's rate of energy expenditure cannot be greater than the cell's rate of energy production. These are fundamental physical constraints that act on any cell growing at a fixed rate.

Underlying these assumptions is an important empirical fact: *E. coli*'s surface area *S* and volume *V* both depend on growth rate. Figure 1A shows experimental measurements of *E. coli*'s length and width at different growth rates and nutrient conditions (Volkmer and Heinemann, 2011). Faster-growing cells are both longer and wider than slower-growing cells (Woldringh et al., 1977; Osborn and Rothfield, 2007; Volkmer and Heinemann, 2011). To compute the surface area and volume of the cell (variables governing energy production capacity and expenditure rate), we use the approximation that the cell is cylindrical with hemispherical ends. The resulting surface-to-volume (*S*/*V*) ratio of the cell computed using these measured lengths and widths is plotted in Figure 1A. These results show a significant 30%–40% reduction in *E. coli*'s *S*/*V* as growth rate increases over the range shown. In the sections below, we use these values of *S* and *V* to reason about the microscopic factors that affect the cell's energy balance and illustrate how our assumptions generate biologically meaningful constraints on cellular metabolism.

Assumption 1. The Cell's Capacity to Produce Energy Is Proportional to the Cell Membrane Surface Area: The Problem of Glucose Uptake

Figure 1B shows how glucose and other nutrients are taken up by *E. coli* in two steps: (1) passive diffusion through porin channels in the outer membrane, followed by (2) active uptake by transporters in the inner membrane. Transport through outer membrane porins plays a critical part in uptake kinetics (Koch and Wang, 1982). Diffusion of nutrients through their water-filled pore can be modeled using the Renkin-modified diffusion equation (Renkin, 1954; Nikaido and Rosenberg, 1981). This equation relates the rate of influx to measurable physical quantities such as pore diameter, depth, and abundance, as well as the effective diameter of the nutrient. Using this model, the uptake rates of nutrients varying in size from lactose to glucose to glycerol were shown to be consistent with a diffusive bottleneck through pores with a diameter of 1.2 nm (Nikaido and Rosenberg, 1981), consistent with the size of porin channels (Nikaido and Rosenberg, 1983). We compute the permeability of the *E. coli* outer membrane to glucose as roughly 3 μm/s (Table S1A). While permeability could be increased by expanding the pore diameter, this has been observed to increase sensitivity to toxins, suggesting that porins also play a protective role for the cell (Kojima and Nikaido, 2013).

The second step of glucose uptake is through inner membrane transporters. We estimate that glucose transporters occupy only 1% of the membrane area when overflow metabolism begins, and thus make a much smaller contribution to inner membrane crowding than the electron transport chain (Figure 2A and Box 1). This number is obtained using the area of a glucose

Box 1. Membrane Requirements of ATP Production

Respiration and acetate fermentation are the two major routes to ATP generation in *E. coli* grown aerobically on glucose (Neidhardt and Curtiss, 1996). While *E. coli* can perform several different kinds of fermentation, acetate is the predominant end product of overflow metabolism in glucose media (Valgepea et al., 2011; O'Brien et al., 2013). ATP generation by both routes can be divided into electron transport chain-dependent and electron transport chain-independent parts. This is shown in the Figure B1, where α represents the number of ATP produced independently of the electron transport chain, while n represents the number of NADH equivalents produced that are used by the electron transport chain to generate ATP (Table S1C).

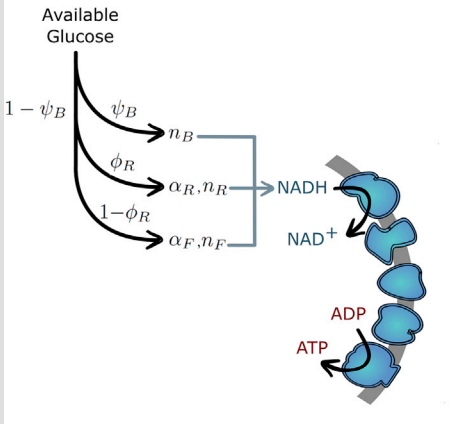

	NDH-I	SDH	Cyo	Cyd-I	ATP synthase
Stoichiometry	1/4	1	1/3	1/4	1
Membrane area (nm²)	80	10	35	30	35
Per respiratory unit (nm²)	20	10	12	7	35

* NDH-I = NADH dehydrogenase I; SDH = succinate dehydrogenase; Cyo = cytochrome *bo* terminal oxidase; Cyd-I = cytochrome *bd*-I terminal oxidase.

ATP source	ATP rate (ATP/s)	Membrane area (nm²)	Surface efficiency (ATP/s/nm²)
ETC-independent	720	48	15
ETC-dependent	270	84	3

Metabolic mode	ETC-independent surface efficiency (ATP/s/nm²)	ETC-dependent surface efficiency (ATP/s/nm²)	Total surface efficiency (ATP/s/nm²)
Acetate Fermentation	15	-	15
Respiration	15	3	4

Figure B1. Acetate Fermentation Is More Surface-Efficient than Respiration

(Left) NADH and ATP production depends on how glucose is partitioned between biomass production, acetate fermentation, and respiration. NADH is consumed by the electron transport chain to produce ATP. Top right: membrane real estate occupied per electron transport chain complex and per respiratory unit, normalizing to ATP synthase. Middle right: surface efficiency of electron transport chain (ETC)-independent energy generation (transporter + cytosolic processes) and ETC-dependent processes (only ETC). Bottom right: the net surface efficiency of each metabolic mode depends on its component efficiencies. Our calculations assume a phosphate/oxygen (*P/O*) ratio of 1.0 (Hempfling and Mainzer, 1975; Farmer and Jones, 1976; Noguchi et al., 2004; Feist et al., 2007) for conversion of NADH to ATP via the electron transport chain (Tables S1A and S1B).

For each part, we can define surface efficiency as the number of ATP/s produced from a given amount of membrane area. The electron transport chain-independent part requires only glucose transporters (48 ± 10 nm^2/dimer), which can supply a maximum of 180 ± 40 glucose/s that each yield 4 ATP in both respiration and acetate fermentation. This gives a surface efficiency of 15 ± 5 ATP/s/nm^2. The surface efficiency of the electron transport chain-dependent part can be estimated from experimental electron transport chain protein structures, abundances, and kinetics (Valgepea et al., 2013; Etzold et al., 1997). Normalizing abundances to the terminal ATP synthase, an estimated 84 nm^2 of electron transport chain is required to generate 270 ± 40 ATP/s, the maximum speed of ATP synthase (Etzold et al., 1997), resulting in a surface efficiency of only 3 ± 1 ATP/s/nm^2 (Tables S1B and S1D). The electron transport chain stoichiometry shown in the table below represents averages across growth rates (Valgepea et al., 2013) (Table S1B).

A key conclusion from these calculations is that the larger number of NADH equivalents produced from acetyl-CoA by the TCA cycle (7.2 , Table S1C [Alberts et al., 2002]) compared with acetate fermentation (0) is both the source of respiration's greater ATP yield *and* its lower surface efficiency, as it creates a high demand for surface-inefficient electron transport chain. It therefore follows that once the inner membrane reaches its protein packing limit, the cell can continue to increase its ATP production rate and growth rate by gradually increasing the fraction of glucose directed to acetate fermentation rather than the TCA cycle, as observed experimentally (Vemuri et al., 2006; Valgepea et al., 2011; O'Brien et al., 2013).

transporter dimer (48 ± 10 nm^2) (Jeckelmann et al., 2011), its maximum uptake rate (k_T = 180 ± 40 glucose/s), the surface-to-volume ratio of a cell (Figure 1A), and the cell's total glucose uptake rate (Vemuri et al., 2006; O'Brien et al., 2013) (Table S1A). Thus, while glucose transporters can saturate at high glucose concentrations, the abundance of these transporters can be increased to keep up with the non-saturating influx through porins (Koch and Wang, 1982). As shown in Figure 1B, the net uptake rate R_G through *both* steps can therefore be expressed by the influx through porins, multiplied by the fraction ϕ of glucose molecules diffusing in through porins that are taken up by inner membrane transporters rather than escaping back out into the environment.

Why do cells not express even more inner membrane transporters for a given nutrient concentration? Once inner membrane transporters have become so abundant that the uptake capacities of the two membranes are comparable, there is diminishing value in producing more. This two-step mechanism may also resolve a puzzling observation (Koch and Wang, 1982): glucose uptake and growth rate do not always follow the saturating kinetics expected by Monod (1949). Instead, they can show extremely linear behavior when glucose uptake is rate-limited by the non-saturating process of diffusion through porins, as modeled previously (Koch and Wang, 1982; Nikaido and Rosenberg, 1981).

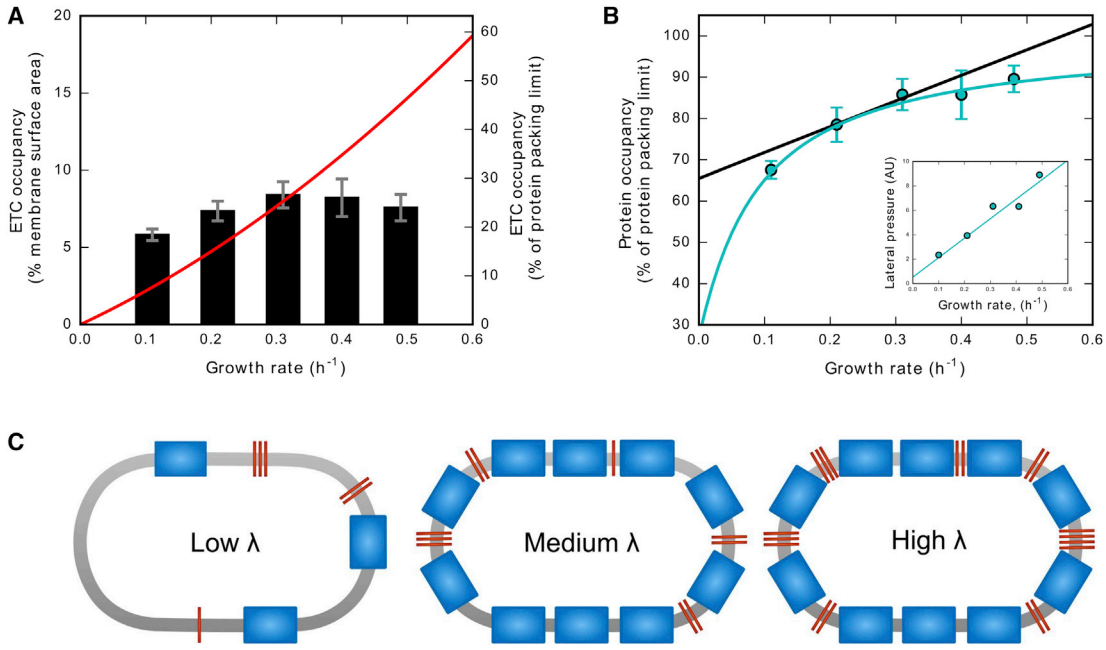

Figure 2. Increasing Demand for ATP Drives Electron Transport Chain Surface Occupancy

(A) Black bars: estimated occupancy of the inner membrane by standard electron transport chain complexes, from experimental data (Valgepea et al., 2013) (Table S1B). Red line: the minimal amount of electron transport chain needed to maintain a purely respiratory metabolism. The crossing point at 0.32 ± 0.10 hr^{-1} indicates that respiration alone is not sufficient to supply the cell's ATP needs above this growth rate, leading to overflow metabolism (Valgepea et al., 2011).

(B) The total inner membrane protein density (cyan points) follows the trend predicted from a Carnahan-Starling model of protein crowding (cyan curve) for a protein packing limit of one-third (fitting parameter, see text). This differs from the density needed to maintain fixed stoichiometry between membrane and cytosolic proteins, approximated here by *V*/*S* (black curve). Inner membrane proteins appear to reach their packing limit concurrently with the onset of fermentation at λ = 0.3 hr^{-1}. Inset: steric pressure from protein crowding increases linearly with growth rate.

(C) Prior to the inner membrane reaching its protein packing limit, both glucose transporters (red) and electron transport chain (blue) have space to increase. But once the packing limit is reached, higher growth rates require increases only in glucose transporters to fuel acetate fermentation due to its greater surface efficiency for generating ATP (see Box 1).

Error bars represent SDs of experimental abundances.

Assumption 2. The Cell's Rate of Energy Demand Is Proportional to the Cell Volume: The Problem of ATP Production

Above, we reasoned about the effect of *S* and *V* on the rate of glucose uptake, that is, the raw material for the cell's energy supply. They are also intimately related to the cell's rate of ATP demand. But how large is this demand and how much membrane space is needed to supply it? We define $R_{ATP\text{-}demand}$ as the number of ATP molecules per unit time, per unit cell volume, that must be produced in order for a cell to sustain a growth rate λ. The amount of ATP, α_B, needed to produce *E. coli* biomass aerobically on glucose is roughly 18 billion ATP molecules per femtoliter of cell volume (Stouthamer and Bettenhaussen, 1977; Hempfling and Mainzer, 1975; Feist et al., 2007) (Table S1A). In this work, our term *ATP* is shorthand that includes all nucleotide triphosphates. To support a growth rate λ, the cell demands ATP at a rate

$$R_{ATP-demand} = \alpha_B \lambda. \qquad \text{(Equation 1)}$$

Now, at steady state, this rate of ATP demand must be met by the rate of ATP supply. For the cell to achieve this via respiration, there is a minimum fraction of the bacterial inner membrane that must be electron transport chain. We can estimate this fraction from the known electron transport chain structural and kinetic properties (Tables S1A and S1B), according to

$$ETC_{demand} = R_{ATP-demand} f_{ETC} \cdot \frac{A_{ETC}}{k_{ATP}} \cdot \frac{V}{S}. \qquad \text{(Equation 2)}$$

f_{ETC} is the fraction of $R_{ATP\text{-}demand}$ generated by the electron transport chain (the remainder by glycolysis and the TCA cycle; Box 1 and Table S1C). This ATP demand can be converted to an electron transport chain surface area by multiplying the first term by the surface efficiency of the electron transport chain, given by A_{ETC}/k_{ATP}. A_{ETC} is the membrane area occupied by a single "respiratory unit," defined as the amount of electron transport chain needed to power a single ATP synthase at its maximum speed k_{ATP} = 270 ± 40 ATP/s (Etzold et al., 1997). The area of a respiratory unit, roughly 84 nm^2, is calculated from the cross-sectional areas of the five electron transport chain complexes' protein structures and their abundances relative to ATP synthase (Box 1; Tables S1B and S1D). The final term accounts for the reasonable assumption that ATP demand for replication scales with the volume *V* of the cell. To express ETC_{demand} as a fraction of total membrane area, we divide by *S*, resulting in Equation 2.

Thus far, we have estimated the membrane demands of the electron transport chain, assuming that ATP is produced by a

purely respiratory metabolism. Would less membrane area be needed if acetate fermentation was used instead? In other words, is acetate fermentation more surface efficient? A detailed calculation of the surface efficiency of both acetate fermentation and respiration can be found in Box 1. We find the membrane efficiency of acetate fermentation to be 15 ± 5 ATP/s/nm^2, significantly higher than respiration's 4 ± 1 ATP/s/nm^2. Acetate fermentation can therefore produce the same amount of ATP as respiration using roughly a quarter of the membrane space, at the expense of a much lower ATP yield per glucose (Neidhardt and Curtiss, 1996) (Box 1).

This observation illustrates the fundamental tension captured in the membrane real estate hypothesis. When sufficient membrane space is available to run on a fully respiratory metabolism, the cell will do so to maximize the flow of glucose to biomass (rather than for ATP) and thus maximize growth rate and yield. However, if membrane space becomes limiting, the cell can only fuel higher growth rates by producing additional ATP through more surface-efficient means, thus beginning overflow metabolism.

Consequences of the Membrane Real Estate Hypothesis

Limits of Respiration

Figure 2 shows a key test of the membrane real estate hypothesis. In *E. coli*, the onset of fermentation typically occurs at growth rates of 0.3–0.5 hr^{-1} (Valgepea et al., 2011; Ishii et al., 2007; Vemuri et al., 2006). But why? Our calculation of the minimal amount of electron transport chain needed to fuel growth, summarized in Equation 2 and shown by the red line in Figure 2A, demonstrates how rapidly the electron transport chain's membrane requirements increase with growth rate, eventually becoming untenable. For comparison, the black bars in Figure 2A show the experimentally measured membrane occupancies of electron transport chain proteins at different growth rates. We determined these occupancies by combining the protein concentrations measured experimentally (Valgepea et al., 2013) with their cross-sectional areas determined from protein structures (Box 1 and Table S1B). The black bars show that faster-growing cells have increased electron transport chain densities in the inner membrane, up to a growth rate of 0.3 hr^{-1}, beyond which densities roughly plateau. The mild decline in electron transport chain densities above 0.3 hr^{-1} is thought to be from competition with glucose transporters (Zhuang et al., 2011) and other growth-related functions (Box 1). Importantly, the saturation in electron transport chain densities is predicted to cause the cell's maximum respiratory capacity (black bars) to cross the line of ATP demand (red curve) at a growth rate of roughly 0.32 ± 0.10 hr^{-1}. This suggests that the cell needs to switch from using pure respiration to a mixture of respiration and acetate fermentation at this growth rate. This is a key prediction of this work and serves as an upper limit for the onset of acetate fermentation, λ_{ferm}, as it assumes the electron transport chain is kinetically saturated. Consistent with the membrane real estate hypothesis, this predicted λ_{ferm} is very close to the onset point of 0.27 hr^{-1} observed by the same group that measured the protein abundances used here (Valgepea et al., 2011, 2013).

Figure 2A also shows the prediction that fermentation begins when electron transport chain complexes occupy 8%–9% of the total inner membrane area. If the membrane real estate hypothesis is valid, then why is the saturating electron transport chain occupancy not 100%? First, the integrity of the membrane requires some minimal number of lipid molecules to solvate each protein complex. Second, the cell could not function without additional, non-electron transport chain membrane proteins. To estimate the absolute membrane occupancy of these non-respiratory proteins, we (1) use data from Valgepea et al. (2013) to determine *relative* abundances of non-electron transport chain proteins at each growth rate and (2) use the independent experimental observation that metabolic functions, predominantly electron transport chain, make up roughly one-third of all inner membrane proteins (Papanastasiou et al., 2013) (Table S1B). Adding this estimate of non-electron transport chain occupancies to the electron transport chain densities in Figure 2A, we determine the membrane crowding for the whole inner membrane proteome, shown in Figure 2B. Like the electron transport chain, total inner membrane crowding appears to reach its limit at a growth rate of roughly 0.3 hr^{-1}, concurrently with the onset of acetate fermentation. This is consistent with the hypothesis that further increases in electron transport chain are limited by membrane crowding.

Driving Forces of Membrane Crowding

What is the mechanism by which proteins become crowded within the inner membrane? What drives electron transport chain concentrations to increase with growth rate at slow growth, then reach a plateau at fast growth? Here is the simplest physical mechanism, we believe, that captures the saturating behavior observed experimentally. At slow growth rates, the cell has sufficiently high *S/V* relative to its metabolic needs that the densities of electron transport chain and other inner membrane proteins can increase with growth rate. However, the densities cannot increase indefinitely, as the increasing steric repulsions between close-packed proteins would limit further protein insertion into the membrane. This simple idea, in which lateral steric repulsion (measured in terms of pressure P) depends on the packing density in the inner membrane, can be expressed by the two-dimensional Carnahan-Starling model (Scalise et al., 1998). By representing membrane proteins as sterically repulsive disks in the two dimensions of the membrane, the Carnahan-Starling model predicts that the pressure P grows as

$$P \propto \eta \left[\frac{1 + c\eta^2}{(1-\eta)^2} \right], \text{ where } c = \frac{7}{3} - \frac{4\sqrt{3}}{\pi}, \qquad \text{(Equation 3)}$$

η is the filling fraction occupied by disks, and c is a packing constant (Scalise et al., 1998). Given that the transmembrane regions of proteins are generally smaller and occupy less lateral space than their solvent-exposed domains adjacent to the membrane (e.g., electron transport chain proteins, transporters, and ribosomes docked to translocation machinery), our calculated membrane occupancies can only be related to η up to a multiplicative "bulbosity" factor that accounts for the steric clash of these much larger bulbous outer regions. Here, we want $\eta(P)$ rather than $P(\eta)$, so we invert the function above. A similar relation has been used previously to assess membrane curvature due to

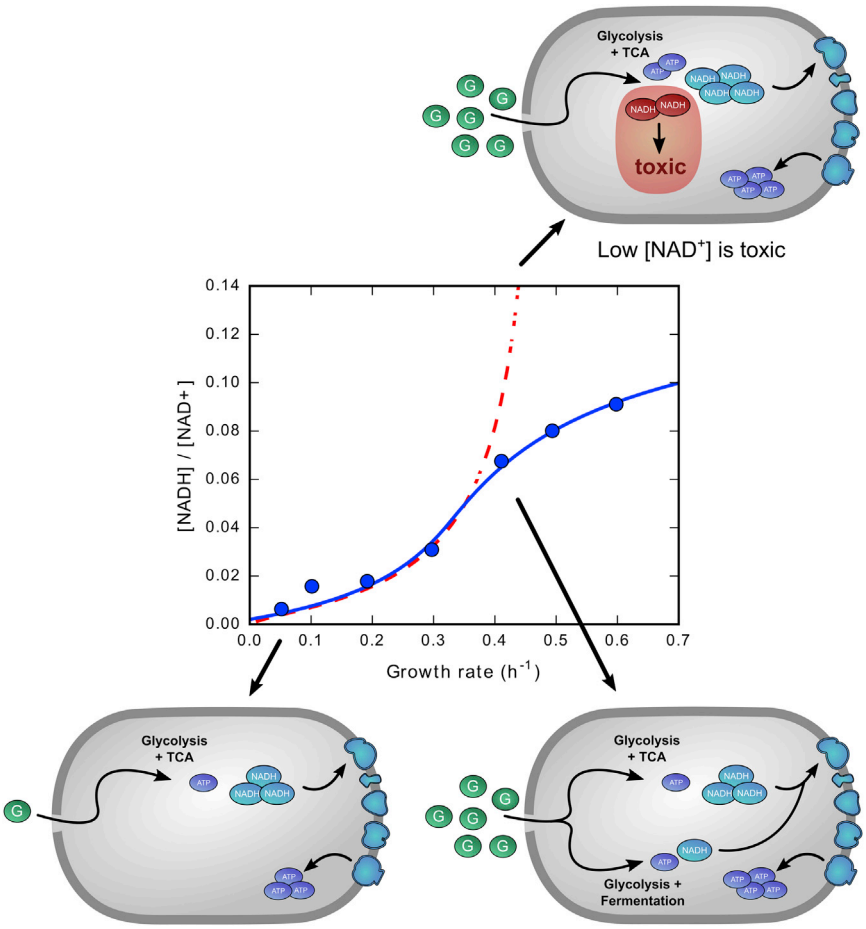

Figure 3. Fermentation Prevents NADH Imbalance

The concentration of NADH depends on the balance between NADH production via glycolysis, the TCA cycle, acetate fermentation, and biomass production, which scales with cell volume, and the consumption of NADH by the electron transport chain, which scales with cell surface area. At low growth rates (bottom left), sufficient electron transport chain exists to keep the [NADH]/[NAD^+] ratio low. At high growth rates, electron transport chain surface limitation would make it impossible to metabolize all of the NADH created, leading to NADH imbalance and potential toxicity due to lack of [NAD^+] (Vemuri et al., 2006; Imai, 2016) (top right; red curve in plot, model). By producing fewer NADH per ATP, fermentation allows the cell to produce sufficient ATP while avoiding NADH imbalance (lower right; experimental points, curve is guide to the eye).

protein packing in unilamellar vesicles (Stachowiak et al., 2012; Scheve et al., 2013).

The Carnahan-Starling model gives an analytical expression for the expected saturation function describing membrane crowding. Like air in a balloon, Equation 3 quantifies the intuition that when few proteins are in the membrane, corresponding to low η, crowding-pressure is very low. As η approaches 1, representing the case where the inner membrane is crammed with proteins, the pressure grows rapidly. Like the balloon, this pressure represents the physical force that would be required to make enough space to insert another protein. In fitting the Carnahan-Starling model to the data, we assume that pressure depends linearly on growth rate.

Figure 2B displays the two main findings. First, the data are consistent with the Carnahan-Starling model in Equation 3 (cyan curve) for a linear $P(\lambda)$ relation (inset). Note that P does not go to zero at $\lambda = 0$ hr^{-1}, as proteins are constantly being degraded and newly inserted, and thus there is a pressure-producing driving force even in the absence of overall growth (the intercept corresponds to a 20-hr protein half-life, albeit with large uncertainty). Second, the fit predicts that membrane proteins behave sterically like objects that are 3-fold larger than their transmembrane region estimated in this work (the bulbosity factor), thus limiting their maximum *membrane* occupancy to one-third. This value is plausible, given that the molecular structures of electron transport chain complexes are, on average, estimated to be 2-fold larger outside the membrane than within it (Table S1B). This bulbous nature of membrane proteins could also resolve why the mitochondrial inner membrane, among the most densely packed ever recorded, is estimated to be "only" around 40% protein within the membrane (Schwerzmann et al., 1986). In summary, despite increasing driving forces, steric crowding appears to limit overall inner membrane protein densities, and thus the electron transport chain content, of an *E. coli* cell. We hope that these intriguing observations will spur future investigations into the nature of these driving forces and their effect on protein insertion.

Predictions of the Membrane Real Estate Hypothesis

The [NADH]/[NAD^+] Ratio

What is the signal that initiates overflow metabolism? We believe it to be the [NADH]/[NAD^+] redox ratio. This ratio is a critical regulator of cell metabolism (Vemuri et al., 2006) in both single cells (Shen and Atkinson, 1970) and multicellular organisms (Imai, 2016), with changes in the [NADH]/[NAD^+] ratio known to be important in both cancer (Vander Heiden et al., 2009; Chiarugi et al., 2012; Fan et al., 2011; Pelicano et al., 2006) and aging (Imai, 2016). A major role of NADH (the reduced form of NAD^+) is to supply electrons to the electron transport chain, driving the production of ATP. The levels of NADH necessary to fuel the electron transport chain are produced in slow-growing cells by glycolysis and the TCA cycle (see the bottom-left cartoon in Figure 3).

Consider two possible fast-growth scenarios. First, suppose there were no membrane limitations. With increasing growth rate, higher production of NADH could be matched by increasing electron transport chain concentration. This would allow NADH levels to remain low. However, in cells *with* surface limitations, while NADH production is proportional to the volume of the cell, the electron transport chain increases only in proportion to

the surface area. So at steady state, NADH concentration would rise sharply. The red dashed curve in Figure 3 shows this expectation. However, high concentrations of NADH are toxic to the cell, because it competes for NAD^+ binding sites, reducing the activities of many enzymes and causing glycolysis to stop (Houtkooper et al., 2010; Shen and Atkinson, 1970). Hence, under surface limitation, purely oxidative respiration would become toxic at high growth rates (top-right cartoon in Figure 3).

To quantitatively test the role of surface limitation in controlling NADH levels, we determine the rise of NADH expected for pure respiration, using a simple binding calculation (the red line in Figure 3). We start with the *S/V* versus growth rate data shown in Figure 1. We assume that electron transport chain densities follow the Carnahan-Starling relation in Figure 2B with a packing limit of approximately 10% of total membrane area, as shown in Figure 2A. Now, if NADH is consumed entirely by the electron transport chain following Michaelis-Menten kinetics (Hayashi et al., 1989), the NADH concentration can be predicted by setting the rate of NADH production equal to its rate of consumption. This gives

$$R_G[(1-\psi_B)n_R+\psi_B n_B]=\frac{k_{\mathrm{NADH}}[\mathrm{ETC}]}{1+K_{\mathrm{NADH}}/[\mathrm{NADH}]}, \qquad \text{(Equation 4)}$$

where ψ_B is the fraction of glucose used for biomass (the remainder used for ATP), n_R and n_B are the numbers of NADH produced per glucose from respiratory and biomass pathways, respectively, and [ETC] is the concentration of respiratory units per cell volume (Box 1). The maximum rate of NADH consumption per respiratory unit, k_{NADH}, is taken to be the maximum rate of ATP synthesis per ATP synthase (270 ATP/s [Etzold et al., 1997]) divided by the phosphate/oxygen ratio (1.0). K_{NADH} is the Michaelis-Menten binding constant of NADH to NADH dehydrogenase I (NDH-I), described below. Rearranging Equation 4 gives

$$[\mathrm{NADH}]=K_{\mathrm{NADH}}\left(\frac{k_{\mathrm{NADH}}[\mathrm{ETC}]}{R_G[(1-\psi_B)(n_R)+\psi_B n_B]}-1\right)^{-1}. \qquad \text{(Equation 5)}$$

The behavior of the [NADH]/[NAD^+] ratio predicted from membrane crowding (Equation 5) is shown by the red curve in Figure 3. This curve is computed using a Michaelis-Menten fit value of K_{NADH} = 74 μM, remarkably close to the experimental estimate of 96.5 μM (Hayashi et al., 1989), given the uncertainly in the underlying parameters. Note that comparison of the [NADH] curve with data on the [NADH]/[NAD^+] ratio requires knowledge of [NAD^+]. Luckily, [NAD^+] has been shown experimentally to be roughly constant across the growth rates studied here (4 mM is used here [Vemuri et al., 2006; Andersen and Meyenburg, 1977]). This minimalist calculation in Equation 5 indicates that the rise in NADH levels is likely a direct consequence of surface limitation, which forces the onset of fermentation to avoid NADH imbalance that would deplete essential [NAD^+] (Vemuri et al., 2006; Imai, 2016).

Now, suppose instead that the cell begins to use acetate fermentation when respiration becomes membrane limited, diverting glucose away from the TCA cycle where much of the NADH is made. As a result, acetate fermentation produces fewer NADH per ATP than respiration does, 1-to-1 compared to 2.5-to-1 (Box 1 and Table S1C). The onset of fermentation thus allows the cell to avoid NADH imbalance while generating the ATP necessary to fuel high growth rates (bottom-right cartoon and blue curve in Figure 3). Acetate fermentation has the further advantage of producing more ATP per glucose than other forms of fermentation (Neidhardt and Curtiss, 1996).

The role of the [NADH]/[NAD^+] ratio in controlling the onset of overflow metabolism is supported by its known roles in regulating the activity of several glycolytic and TCA cycle enzymes (Shen and Atkinson, 1970). Further support comes from the observation that the same triggering ratio is reached in both wild-type *E. coli* and a NOX^+ mutant strain expressing a cytosolic NADH-consuming enzyme (Vemuri et al., 2006). This trigger appears to be controlled by the ArcAB system, which is thought to sense and respond to either the [NADH]/[NAD^+] ratio or the oxidation state of quinones within the respiratory chain (Vemuri et al., 2006). Both are expected to respond similarly to the saturating respiratory kinetics modeled here.

Flexibility of Overflow Metabolism

The present model makes additional predictions, which could be tested experimentally. If the surface-to-volume ratio is indeed a key factor in the fermentation switch, different organisms or strains having different surface-to-volume ratios should have different fermentation onset points, λ_{ferm}. We compute the relationship between the onset point and *S/V* by setting the electron transport chain demand (Equation 2) equal to its maximum membrane occupancy (ETC_{max}). Solving for λ_{ferm} gives

$$\lambda_{ferm}=\left[\frac{1}{\alpha_B f_{ETC}}\cdot\frac{k_{ATP}}{A_{ETC}}\cdot ETC_{max}\right]\frac{S}{V}. \qquad \text{(Equation 6)}$$

Equation 6 predicts that variation in λ_{ferm} can arise from two sources: either through cell-level changes in *S/V* or through changes in the prefactor in brackets. While published data on cell sizes suggest that *S/V* can vary by a factor of 2 between strains (Woldringh et al., 1977; Volkmer and Heinemann, 2011) or within a long-term evolution experiment (Lenski and Travisano, 1994), the variability of the prefactor requires closer attention. First, fundamental costs of biosynthesis (Neidhardt and Curtiss, 1996) would suggest little variation in α_B on a given food source. Similarly, the maximum speed of ATP synthase (k_{ATP}) is likely to be tightly constrained by evolutionary selection. The greatest sources of variation are thus expected to be the inner membrane's maximum electron transport chain fraction (ETC_{max}), the electron transport chain surface area per ATP synthase (A_{ETC}), and the fraction of ATP produced by the electron transport chain (f_{ETC}).

While determination of the degree of variability in the maximum electron transport chain fraction, ETC_{max}, will require future experiments, we can estimate the extent of variation allowed in f_{ETC} and A_{ETC} from existing data. First, the fraction of ATP derived from the electron transport chain (f_{ETC}) depends on the number of ATP produced per NADH equivalent. This number, called the phosphate/oxygen (*P/O*) ratio, is a measure of electron transport chain energy efficiency. If *P/O* = 1 (1 ATP per NADH), as measured experimentally (Hempfling and Mainzer, 1975), f_{ETC} is simply the number of NADH equivalents produced per glucose (11.2; Box 1) divided by the total amount of ATP produced (4 + 11.2), giving f_{ETC} = 0.74. For *P/O* = 2, these

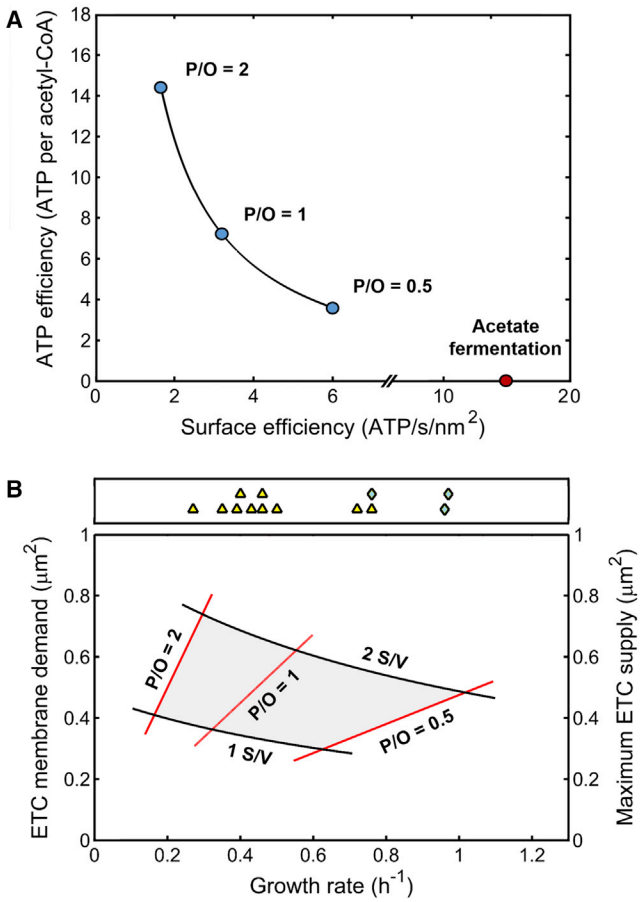

Figure 4. Efficiency Trade-Offs Are Predicted to Affect the Growth Rate at which Overflow Metabolism Begins

(A) Isoforms of NADH dehydrogenase (NDH-I and NDH-II) and terminal oxidases (Cyo, Cyd-I, and Cyd-II) give the cell flexibility to adapt the respiratory chain's surface efficiency (ATP/s per membrane area) and ATP efficiency (ATP per acetyl-CoA) along a speed-efficiency Pareto surface. The position along this surface can be defined by the phosphate/oxygen (*P/O*) ratio, a measure of respiratory efficiency.

(B) The flexibility in electron transport chain efficiency, when combined with the observed variation in *S/V*, results in a range of possible growth rates at which the demand for ATP exceeds the electron transport chain's capacity (shaded region). The minimum and maximum *P/O* ratios of 0.5 and 2 define the right and left boundaries of the allowed region, while the central line shows the demand for the *P/O* value of 1 observed experimentally (Hempfling and Mainzer, 1975; Farmer and Jones, 1976; Noguchi et al., 2004; Feist et al., 2007) and used in this work. Likewise, the *S/V* values in Figure 1 (among the largest measured) and double this value (among the smallest [Woldringh et al., 1977]) constrain the electron transport chain capacities to the lower and upper boundaries of the shaded region. This region predicts the range of growth rates λ_{ferm} at which overflow metabolism is expected to begin. This flexibility may underlie the large variation in λ_{ferm} observed experimentally (yellow triangles) (Meyer et al., 1984; Holms, 1996; Feist et al., 2007; Nanchen et al., 2006; Vemuri et al., 2006; Nahku et al., 2010; Peebo et al., 2015; Ishii et al., 2007; Renilla et al., 2012; Basan et al., 2015) and makes a prediction for the phenotype of three strains that do not ferment (blue diamonds) (Monk et al., 2016).

numbers would be 22.4 and 26.4, giving f_{ETC} = 0.85 (Table S1C). Thus the higher the *P/O* ratio, the greater the fraction of ATP produced by the electron transport chain. Given that ATP synthase is already working at close to maximum speed at the onset of fermentation (Figure 2A), the required number of electron transport chain units under a fully respiratory metabolism should therefore increase with f_{ETC}.

Second, for A_{ETC}, *E. coli* is known to have isoforms of both NADH dehydrogenase (NDH-I and NDH-II) and the terminal oxidases (Cyo, Cyd-I, and Cyd-II) that have greater speeds per unit membrane area, at the expense of pumping fewer protons and thus producing fewer ATP per NADH (Zhuang et al., 2011; Feist et al., 2007). In light of our estimate that NADH dehydrogenases and terminal oxidases in total account for roughly half of the electron transport chain's membrane occupancy (Box 1), the fast isoforms are unlikely to increase the surface efficiency of the electron transport chain by more than a factor of two, even if the isoforms were infinitely small or fast (Table S1B). Note that the use of these less efficient isoforms is a major cause for lower *P/O* ratios; hence f_{ETC} and A_{ETC} are expected to covary.

The trade-off in expressing these different electron transport chain isoforms can be seen by defining two types of efficiency: the effectiveness of producing high amounts of ATP from glucose (ATP efficiency) and the effectiveness at utilizing membrane area (surface efficiency). This trade-off is shown as a Pareto surface in Figure 4A (Tables S1B and S1C). Moving toward the upper left the cell gets more ATP per glucose at the expense of lower surface surface efficiency, while moving toward the bottom right gives more efficient usage of membrane space but a lower ATP yield per glucose.

By changing its position along this Pareto surface, a cell can alter its fermentation onset point, as shown by Equation 6. This may have enabled the large variation in published values of λ_{ferm} to evolve (Meyer et al., 1984; Holms, 1996; Feist et al., 2007; Nanchen et al., 2006; Vemuri et al., 2006; Nahku et al., 2010; Peebo et al., 2015; Ishii et al., 2007; Renilla et al., 2012; Basan et al., 2015; Monk et al., 2016). By inserting the range of possible values of f_{ETC} and A_{ETC} into ETC_{demand}, together with the experimental range of *S/V*, Equation 6 allows us to predict the range of possible values of λ_{ferm} that different strains could explore. Not only does the predicted range, shown by the shaded region in Figure 4B, capture the inter-strain variability in λ_{ferm} (triangles), it also makes a statement about three exceptions. A recent study of different *E. coli* strains found that three do not ferment, even at the fastest growth rates on glucose minimal medium (Monk et al., 2016) (diamonds in Figure 4B). From molecular data, our model suggests that these strains are at the edge of the possible onset region. By residing at the right corner of the shaded region, our model makes the further predictions that these strains, together with those possessing very high λ_{ferm}, must rely heavily on the fast, inefficient isoforms of the electron transport chain, have low *P/O* ratios, and be small in size, permitting large *S/V*.

The shaded region can also be shifted by other means. Overexpression of non-respiratory inner membrane proteins is predicted to move this shaded region by effectively decreasing the available *S/V*. This causes fermentation to be triggered at lower growth rates, as observed experimentally (Wagner et al., 2007). A key prediction that distinguishes the membrane real estate hypothesis from other models (Basan et al., 2015) is that it predicts that λ_{ferm} is more sensitive to the overexpression of "dummy" proteins that reside in the inner membrane rather than the cytosol, as the former directly competes with the electron transport chain for membrane space. Unfortunately, aggregation and membrane leakage have made verification of this

prediction experimentally challenging (Wagner et al., 2007). Nonetheless, we hope that the model's targeted predictions motivate future experimental testing.

Finally, why did *E. coli* not evolve a larger *S/V* ratio? We do not know, but several lines of evidence suggest that larger *S/V* surely has fitness penalties too. First, it has been estimated that *E. coli* spends up to half of its energy maintaining ion gradients across a leaky inner membrane (Stouthamer and Bettenhaussen, 1977), with this leakiness plausibly increasing as *S/V*. Second, surface structures account for roughly one-third of *E. coli*'s dry mass, consisting of inner and outer membrane proteins, lipids, and carbohydrates, much greater than the 1%–2% of dry mass in electron transport chain (Neidhardt and Curtiss, 1996; Basan et al., 2015). Thus, *if* the inner membrane does indeed reach its protein packing limit, as our analysis suggests, it follows that any increases in *S/V* for the purpose of increased respiration comes at a cost many times greater than just the synthesis of the electron transport chain. Such considerations imply that *E. coli*'s *S/V* constrains its respiration, rather than the reverse.

Conclusions

We have explored here how physical properties of proteins constrain bacterial "decisions" about how best to generate energy. *E. coli* and other cells use inefficient metabolism when growing fast. Even when oxygen is present, cells switch from respiration (which is ATP-efficient) to using fermentation for additional ATP (which is ATP-inefficient). What is the fundamental cause of this puzzling switching? We make numerical estimates indicating that this behavior is consistent with limitations in membrane surface area. For sufficiently fast growth, the ATP demands of the cell exceed the available membrane space to house respiratory complexes. This limitation requires that additional ATP be produced through acetate fermentation, as this produces several-fold more ATP per unit membrane area. This membrane real estate hypothesis is consistent with multiple lines of evidence, including the observation that both membrane protein packing and electron transport chain kinetics reach their respective limits concurrently with the onset of fermentation. Furthermore, the membrane real estate hypothesis suggests that the sharp rise in the [NADH]/[NAD^+] ratio at the onset of overflow metabolism is the direct result of surface limitation and acts as a signal that triggers overflow metabolism to avoid NADH imbalance. The onset of fermentation thus serves as an example of how a cell's behavior and evolution are limited by the physical sizes and shapes of its proteins.

SUPPLEMENTAL INFORMATION

Supplemental Information includes one table and can be found with this article online at http://dx.doi.org/10.1016/j.cels.2017.06.005.

ACKNOWLEDGMENTS

We appreciate the support of the Laufer Center for Physical and Quantitative Biology. We thank Ron Milo, Jorg Schwender, Gabor Balazsi, Dan Bogenhagen, Arijit Maitra, and Purushottam Dixit for very helpful comments.

REFERENCES

Alberts, B., Johnson, A., Lewis, J., Raff, M., Roberts, K., and Walter, P. (2002). Molecular Biology of the Cell, Fourth Edition (Garland Science).

Andersen, K.B., and Meyenburg, K.V. (1977). Charges of nicotinamide adenine-nucleotides and adenylate energy-charge as regulatory parameters of metabolism in *Escherichia coli*. J. Biol. Chem. *252*, 4151–4156.

Andersen, K.B., and Meyenburg, K.V. (1980). Are growth-rates of *Escherichia coli* in batch cultures limited by respiration. J. Bacteriol. *144*, 114–123.

Basan, M., Hui, S., Okano, H., Zhang, Z., Shen, Y., Williamson, J.R., and Hwa, T. (2015). Overflow metabolism in *Escherichia coli* results from efficient proteome allocation. Nature *528*, 99–104.

Chiarugi, A., Dolle, C., Felici, R., and Ziegler, M. (2012). The NAD metabolome—a key determinant of cancer cell biology. Nat. Rev. Cancer *12*, 741–752.

Etzold, C., DeckersHebestreit, G., and Altendorf, K. (1997). Turnover number of *Escherichia coli* f0f1 ATP synthase for ATP synthesis in membrane vesicles. Eur. J. Biochem. *243*, 336–343.

Fan, J., Hitosugi, T., Chung, T.W., Xie, J., Ge, Q., Gu, T.L., Polakiewicz, R.D., Chen, G.Z., Boggon, T.J., Lonial, S., et al. (2011). Tyrosine phosphorylation of lactate dehydrogenase A is important for NADH/NAD(+) redox homeostasis in cancer cells. Mol. Cell. Biol. *31*, 4938–4950.

Farmer, I.S., and Jones, C.W. (1976). Energetics of Escherichia-coli during aerobic growth in continuous culture. Eur. J. Biochem. *67*, 115–122.

Feist, A.M., Henry, C.S., Reed, J.L., Krummenacker, M., Joyce, A.R., Karp, P.D., Broadbelt, L.J., Hatzimanikatis, V., and Palsson, B.Ø. (2007). A genome-scale metabolic reconstruction for *Escherichia coli* K-12 MG1655 that accounts for 1260 ORFs and thermodynamic information. Mol. Syst. Biol. *3*, 121.

Flamholz, A., Noor, E., Bar-Even, A., Liebermeister, W., and Milo, R. (2013). Glycolytic strategy as a tradeoff between energy yield and protein cost. Proc. Natl. Acad. Sci. USA *110*, 10039–10044.

Hayashi, M., Miyoshi, T., Takashina, S., and Unemoto, T. (1989). Purification of NADH-ferricyanide dehydrogenase and NADH-quinone reductase from *Escherichia coli* membranes and their roles in the respiratory chain. Biochim. Biophys. Acta *977*, 62–69.

Hempfling, W.P., and Mainzer, S.E. (1975). Effects of varying the carbon source limiting growth on yield and maintenance characteristics of *Escherichia coli* in continuous culture. J. Bacteriol. *123*, 1076–1087.

Holms, H. (1996). Flux analysis and control of the central metabolic pathways in *Escherichia coli*. FEMS Microbiol. Rev. *19*, 85–116.

Houtkooper, R.H., Canto, C., Wanders, R.J., and Auwerx, J. (2010). The secret life of NAD+: an old metabolite controlling new metabolic signaling pathways. Endocr. Rev. *31*, 194–223.

Imai, S.-I. (2016). The NAD World 2.0: the importance of the inter-tissue communication mediated by NAMPT/NAD+/SIRT1 in mammalian aging and longevity control. NPJ Syst. Biol. Appl. *2*, 16018.

Ishii, N., Nakahigashi, K., Baba, T., Robert, M., Soga, T., Kanai, A., Hirasawa, T., Naba, M., Hirai, K., and Hoque, A. (2007). Multiple high-throughput analyses monitor the response of *E-coli* to perturbations. Science *316*, 593–597.

Jeckelmann, J.M., Harder, D., Mari, S.A., Meury, M., Ucurum, Z., Muller, D.J., Erni, B., and Fotiadis, D. (2011). Structure and function of the glucose PTS transporter from *Escherichia coli*. J. Struct. Biol. *176*, 395–403.

Kayser, A., Weber, J., Hecht, V., and Rinas, U. (2005). Metabolic flux analysis of *Escherichia coli* in glucose-limited continuous culture. I. Growth-rate-dependent metabolic efficiency at steady state. Microbiology *151* (Pt 3), 693–706.

Koch, A.L., and Wang, C.H. (1982). How close to the theoretical diffusion limit do bacterial uptake systems function? Arch. Microbiol. *131*, 36–42.

Kojima, S., and Nikaido, H. (2013). Permeation rates of penicillins indicate that *Escherichia coli* porins function principally as nonspecific channels. Proc. Natl. Acad. Sci. USA *110*, E2629–E2634.

Lenski, R.E., and Travisano, M. (1994). Dynamics of adaptation and diversification: a 10,000-generation experiment with bacterial populations. Proc. Natl. Acad. Sci. USA *91*, 6808–6814.

Meyer, H.-P., Leist, C., and Fiechter, A. (1984). Acetate formation in continuous culture of *Escherichia coli* K12 d1 on defined and complex media. J. Biotechnol. *1*, 355–358.

Molenaar, D., van Berlo, R., de Ridder, D., and Teusink, B. (2009). Shifts in growth strategies reflect tradeoffs in cellular economics. Mol. Syst. Biol. *5*, 323.

Monk, J.M., Koza, A., Campodonico, M.A., Machado, D., Seoane, J.M., Palsson, B.O., Herrgård, M.J., and Feist, A.M. (2016). Multi-omics quantification of species variation of *Escherichia coli* links molecular features with strain phenotypes. Cell Syst. *3*, 238–251.

Monod, J. (1949). The growth of bacterial cultures. Annu. Rev. Microbiol. *3*, 371–394.

Nahku, R., Valgepea, K., Lahtvee, P.J., Erm, S., Abner, K., Adamberg, K., and Vilu, R. (2010). Specific growth rate dependent transcriptome profiling of *Escherichia coli* K12 MG1655 in accelerostat cultures. J. Biotechnol. *145*, 60–65.

Nanchen, A., Schicker, A., and Sauer, U. (2006). Nonlinear dependency of intracellular fluxes on growth rate in miniaturized continuous cultures of *Escherichia coli*. Appl. Environ. Microbiol. *72*, 1164–1172.

Neidhardt, F.C., and Curtiss, R. (1996). *Escherichia coli* and Salmonella: Cellular and Molecular Biology, Second Edition (ASM Press).

Nikaido, H., and Rosenberg, E.Y. (1981). Effect on solute size on diffusion rates through the transmembrane pores of the outer membrane of *Escherichia coli*. J. Gen. Physiol. *77*, 121–135.

Nikaido, H., and Rosenberg, E.Y. (1983). Porin channels in *Escherichia coli*: studies with liposomes reconstituted from purified proteins. J. Bacteriol. *153*, 241–252.

Noguchi, Y., Nakai, Y., Shimba, N., Toyosaki, H., Kawahara, Y., Sugimoto, S., and Suzuki, E. (2004). The energetic conversion competence of *Escherichia coli* during aerobic respiration studied by 31P NMR using a circulating fermentation system. J. Biochem. *136*, 509–515.

Noor, E., Bar-Even, A., Flamholz, A., Reznik, E., Liebermeister, W., and Milo, R. (2014). Pathway thermodynamics highlights kinetic obstacles in central metabolism. PLoS Comput. Biol. *10*, e1003483.

O'Brien, E.J., Lerman, J.A., Chang, R.L., Hyduke, D.R., and Palsson, B.O. (2013). Genome-scale models of metabolism and gene expression extend and refine growth phenotype prediction. Mol. Syst. Biol. *9*, 693.

Osborn, M.J., and Rothfield, L. (2007). Cell shape determination in *Escherichia coli*. Curr. Opin. Microbiol. *10*, 606–610.

Papanastasiou, M., Orfanoudaki, G., Koukaki, M., Kountourakis, N., Sardis, M.F., Aivaliotis, M., Karamanou, S., and Economou, A. (2013). The *Escherichia coli* peripheral inner membrane proteome. Mol. Cell. Proteomics *12*, 599–610.

Peebo, K., Valgepea, K., Maser, A., Nahku, R., Adamberg, K., and Vilu, R. (2015). Proteome reallocation in *Escherichia coli* with increasing specific growth rate. Mol. Biosyst. *11*, 1184–1193.

Pelicano, H., Xu, R.H., Du, M., Feng, L., Sasaki, R., Carew, J.S., Hu, Y., Ramdas, L., Hu, L., Keating, M.J., et al. (2006). Mitochondrial respiration defects in cancer cells cause activation of Akt survival pathway through a redox-mediated mechanism. J. Cell Biol. *175*, 913–923.

Renilla, S., Bernal, V., Fuhrer, T., Castano-Cerezo, S., Pastor, J.M., Iborra, J.L., Sauer, U., and Canovas, M. (2012). Acetate scavenging activity in *Escherichia coli*: interplay of acetyl-CoA synthetase and the PEP-glyoxylate cycle in chemostat cultures. Appl. Microbiol. Biotechnol. *93*, 2109–2124.

Renkin, E.M. (1954). Filtration, diffusion, and molecular sieving through porous cellulose membranes. J. Gen. Physiol. *38*, 225–243.

Scalise, O.H., Zarragoicoechea, G.J., Gonzalez, L.E., and Silbert, M. (1998). Phase equilibria of the two-dimensional Lennard-Jones fluid: reference systems and perturbation theories. Mol. Phys. *93*, 751–755.

Scheve, C.S., Gonzales, P.A., Momin, N., and Stachowiak, J.C. (2013). Steric pressure between membrane-bound proteins opposes lipid phase separation. J. Am. Chem. Soc. *135*, 1185–1188.

Schwerzmann, K., Cruz-Orive, L.M., Eggman, R., Sanger, A., and Weibel, E.R. (1986). Molecular architecture of the inner membrane of mitochondria from rat liver: a combined biochemical and stereological study. J. Cell Biol. *102*, 97–103.

Shen, L.C., and Atkinson, D.E. (1970). Regulation of pyruvate dehydrogenase from *Escherichia coli*. Interactions of adenylate energy charge and other regulatory parameters. J. Biol. Chem. *245*, 5974–5978.

Stachowiak, J.C., Schmid, E.M., Ryan, C.J., Ann, H.S., Sasaki, D.Y., Sherman, M.B., Geissler, P.L., Fletcher, D.A., and Hayden, C.C. (2012). Membrane bending by protein-protein crowding. Nat. Cell Biol. *14*, 944–949.

Stouthamer, A.H., and Bettenhaussen, C.W. (1977). A continuous culture study of an ATPase-negative mutant of *Escherichia coli*. Arch. Microbiol. *113*, 185–189.

Valgepea, K., Adamberg, K., and Vilu, R. (2011). Decrease of energy spilling in *Escherichia coli* continuous cultures with rising specific growth rate and carbon wasting. BMC Syst. Biol. *5*, 106.

Valgepea, K., Adamberg, K., Seiman, A., and Vilu, R. (2013). *Escherichia coli* achieves faster growth by increasing catalytic and translation rates of proteins. Mol. Biosyst. *9*, 2344–2358.

Vander Heiden, M.G., Cantley, L.C., and Thompson, C.B. (2009). Understanding the Warburg effect: the metabolic requirements of cell proliferation. Science *324*, 1029–1033.

van Rijsewijk, B., Nanchen, A., Nallet, S., Kleijn, R.J., and Sauer, U. (2011). Large-scale C-13-flux analysis reveals distinct transcriptional control of respiratory and fermentative metabolism in *Escherichia coli*. Mol. Syst. Biol. *7*, 477.

Vazquez, A., Beg, Q.K., Demenezes, M.A., Ernst, J., Bar-Joseph, Z., Barabasi, A.-L., Boros, L.G., and Oltvai, Z.N. (2008). Impact of the solvent capacity constraint on *E. coli* metabolism. BMC Syst. Biol. *2*, 7.

Vazquez, A., Liu, J., Zhou, Y., and Oltvai, Z.N. (2010). Catabolic efficiency of aerobic glycolysis: the Warburg effect revisited. BMC Syst. Biol. *4*, 58.

Vemuri, G.N., Altman, E., Sangurdekar, D.P., Khodursky, A.B., and Eiteman, M.A. (2006). Overflow metabolism in *Escherichia coli* during steady-state growth: transcriptional regulation and effect of the redox ratio. Appl. Environ. Microbiol. *72*, 3653–3661.

Volkmer, B., and Heinemann, M. (2011). Condition-dependent cell volume and concentration of *Escherichia coli* to facilitate data conversion for systems biology modeling. PLoS One *6*, e23126.

Wagner, S., Baars, L., Ytterberg, A.J., Klussmeier, A., Wagner, C.S., Nord, O., Nygren, P.A., van Wijk, K.J., and de Gier, J.-W. (2007). Consequences of membrane protein overexpression in *Escherichia coli*. Mol. Cell. Proteomics *6*, 1527–1550.

Woldringh, C.L., de Jong, M.A., van den Berg, W., and Koppes, L. (1977). Morphological analysis of the division cycle of two *Escherichia coli* substrains during slow growth. J. Bacteriol. *131*, 270–279.

Zhuang, K., Vemuri, G.N., and Mahadevan, R. (2011). Economics of membrane occupancy and respiro-fermentation. Mol. Syst. Biol. *7*, 500.